Enhancing Open-Circuit Voltage in Gradient Organic Solar Cells by Rectifying Thermalization Losses

Olof Andersson and Martijn Kemerink

In virtually all solar cells, including optimized ones that operate close to the Shockley–Queisser (SQ) limit, thermalization losses are a major, efficiency-limiting factor. In typical bulk heterojunction organic solar cells, the loss of the excess energy of photocreated charge carriers in the disorder-broadened density of states is a relatively slow process that for commonly encountered disorder values takes longer than the charge extraction time. Herein, it is demonstrated by numerical modeling that this slow relaxation can be rectified by means of a linear gradient in the donor:acceptor ratio between anode and cathode. For experimentally relevant parameters, open-circuit voltage (V_{OC}) enhancements up to $\approx$0.2 V in combination with significant enhancements in fill factor as compared to devices without gradient are found. The V_{OC} enhancement can be understood in terms of a simple nonequilibrium effective temperature model. Implications for existing and future organic photovoltaics (OPV) devices are discussed.

1. Introduction

Thermalization of charge carriers is one of the major loss mechanisms in solar cells. When a photon with an energy E_{ph} exceeding the semiconductor bandgap E_{gap} is absorbed, the excess energy $E_{ph} - E_{gap}$ is typically lost to phonon emission, i.e., heat. Together with the detailed balance concept, the position of E_{gap} with respect to the incident light spectrum determines the Shockley–Queisser (SQ) limit, i.e., maximum possible solar-to-electric power conversion efficiency for a single pn

O. Andersson, Prof. M. Kemerink
Complex Materials and Devices
Department of Physics, Chemistry and Biology (IFM)
Linköping University
SE-581 83 Linköping, Sweden
E-mail: martijn.kemerink@cam.uni-heidelberg.de

Prof. M. Kemerink
Centre for Advanced Materials
University of Heidelberg
D-69120 Heidelberg, Germany

The ORCID identification number(s) for the author(s) of this article can be found under https://doi.org/10.1002/solr.202000400.

junction operating near thermodynamic equilibrium.[1] To reduce thermalization losses, so-called hot-carrier solar cells (HCSCs) have been proposed.[2] The concept is based on the collection of charge carriers before equilibration to the band edges has completed. Furthermore, functional HCSCs would enable the use of absorbers with smaller bandgaps, which would improve the total fraction of the solar spectrum that is absorbed. However, achieving HCSCs is complex as it requires, for semiconductors with band transport, the efficiency of elastic carrier–carrier scattering to surpass that of inelastic carrier–phonon scattering to slow down the cooling of charge carriers with respect to the (diffusive) charge extraction process around V_{OC} and to establish an effective charge carrier temperature that exceeds the lattice temperature. However, in most inorganic semiconductors, phonon scattering is very efficient, with typical times in the picosecond range.[2–4] As a consequence, efficient HCSC devices are yet to be realized.[3,4]

Thermalization losses are even more significant in organic photovoltaics (OPV), where one has to distinguish between on-site and global thermalization. The former is similar to inorganic semiconductors and involves the excitation of molecular vibrations till the photocreated charge carrier has adopted the lattice temperature of the (localized) site on which it resides; this process completes on the (sub) picosecond timescale.[5,6] The latter thermalization process is fundamentally different from inorganic solar cells. Due to the combination of strong localization and the presence of large diagonal disorder, charges have to move between localized sites (by thermally activated tunneling or hopping) to thermalize in the density of states (DOS).[7] It has been shown that, due to the latter process, photogenerated charge carriers in OPV continue to lose energy until they are collected at the contacts.[8] The energy losses associated with thermalization in the DOS depend on the, typically Gaussian, width of the DOS and fall in the range of 0.1–0.3 eV for both electrons and holes.[8] In principle, these thermalization losses can be partially mitigated by a strongly enhanced, transient mobility of the charge-carriers in OPV that would facilitate the extraction process. However, transport during the time period immediately after photogeneration is primarily diffusive as a consequence of which most of the energy is lost without any useful contribution to charge-carrier extraction.[8,9] Rectification of the mentioned diffusive motion would therefore be expected to lead to a hot-carrier organic solar cell, where the "hotness" of the charge carriers stems from their incomplete

thermalization in the disorder-broadened distribution of localized sites.

OPV devices are commonly made by blending electron donor and acceptor materials in a given ratio to form a bulk heterojunction (BHJ) active layer. Our hypothesis is that a composition gradient of donor and acceptor materials between anode and cathode will rectify the diffusive motion discussed earlier and mitigate the associated energy losses. Equivalently, in terms of concepts commonly used in the OPV field, a composition gradient may improve charge separation, suppress diffusion of holes and electrons to the wrong contacts, and promote charge transport by exploiting the hotness of photocreated charge carriers by directing the otherwise stochastic hole (electron) motion toward the side with highest donor (acceptor) concentration. This would in turn lead to increased open-circuit voltages (V_{OC}) and fill factors.

In previous literature, gradient vertical phase compositions of donor and acceptor material have been achieved experimentally in various ways, including coevaporation,[10–12] solvent-control,[13] inverted cells,[14] in situ polymerization,[15] inverted off-center spinning,[16] and by introducing a third material in the form of a second acceptor.[17] Although these studies do not reach unanimous results, most of them demonstrate at least a small improvement for a graded composition compared to a nongraded one. Chen et al. investigated fine, multistepped structures of the small molecule system CuPc:C60 and compared varied gradients with the standard bilayer. Fill factor improvement and V_{OC} increases around 0.1 V were obtained; the highest efficiency was obtained for the largest gradient 100:0 which they ascribe to an increased donor/acceptor interface and possibly to a high chemical potential energy gradient.[12] Gradients can also occur unintentionally during layer deposition due to the donor and acceptor materials' different surface energy and solubility, as, e.g., in the study by Guo et al., where the vertical phase gradient is stated to be one reason for the increased V_{OC} and fill factor.[13]

In terms of the formal understanding of gradient composition OPV, to the best of our knowledge, nonequilibrium mechanisms have not been considered and only drift-diffusion-based simulations have so far been reported, at times with the addition of optical modeling.[10,18,19] No clear consensus arises from these simulations. For example, Bi et al. find that for a simulated P3HT/PCBM system, a uniform 50/50 distribution is optimal, although a graded structure with the donor (acceptor) material increasing in a stepped manner toward the anode (cathode) displays a similar (simulated) efficiency.[18] However, also from the simulations of a P3HT:PCBM system, Nam et al. find that charge collection is improved as the donor (acceptor) concentration increases toward the anode (cathode).[19] Crucially, in none of the discussed simulation works, nonequilibrium effects were considered, as would be needed to test our hypothesis. Unlike drift-diffusion models, our kinetic Monte Carlo simulation model, described later, can account for the slow relaxation processes we propose to rectify through composition gradients.

We use the same kinetic Monte Carlo (kMC) model as was previously used for the simulation of transient and steady-state phenomena in BHJ systems.[8,9,20] In short, it uses the extended Gaussian disorder model on a face-centered cubic (fcc) lattice and considers the following: exciton generation and diffusion; charge transfer (CT) pair formation and recombination; electron and hole hopping transport described by the Miller–Abrahams

expression; charge injection/extraction by hopping from/to the Fermi level of the respective contact; full Coulomb interactions, including those by image charges in the electrodes; and periodic boundary conditions in the lateral directions. For maximum transparency of the results, the morphology, that in actual devices may contain complex hierarchical structures of (partially) demixed donor and acceptor phases, was treated in lowest order as a random mixture of individual donor and acceptor sites with a depth-dependent composition. We considered different composition profiles in the z-direction (depth) in our simulations: an abrupt (bilayer) D:A junction; a homogeneous BHJ; linear composition gradients of varying steepness, changing from a donor concentration $c_D = c_{D_0}$ at the anode ($z = 0$) to $c_D = 1 - c_{D_0}$ at the cathode ($z = L$). Therefore, the acceptor concentration $c_A = 1 - c_D$ runs from $1 - c_{D_0}$ to c_{D_0}. We label devices by the donor concentration (in percent) at the anode/cathode, e.g., 70/30 means $c_D = 0.7$ at the anode and $c_D = 0.3$ at the cathode.

Since optimal OPV systems tend to have balanced mobilities, we used equal parameters for electrons and holes throughout this work. The following base parameters were used unless stated otherwise: a Gaussian DOS with highest occupied molecular orbital (HOMO) and lowest unoccupied molecular orbital (LUMO) width of $\sigma_{DOS} = 75$ meV; HOMO/LUMO energy at the donor (acceptor) -3.3 eV/-5.3 eV (-3.7 eV/-5.7 eV) giving an effective bandgap of 1.6 eV; attempt-to-hop-frequency $\nu_0 = 10^{11}$ s^{-1}; lattice temperature $T = 300$ K; and homogeneous generation rate $G_0 = 3 \times 10^{28}$ m^{-3}s^{-1} ($\approx$3 Sun, to improve signal-to-noise). The simulation box size was $50 \times 50 \times 50$ sites with a nearest neighbor hopping distance $a_{NN} = 1.8$ nm, corresponding to an active layer thickness of $L = 74$ nm. We used a fcc lattice, see Figure S1, Supporting Information, for further information. These parameters represent realistic numbers as found in previous works while keeping computation times reasonable. Anode and cathode injection barriers were set to 0.3 eV to give built-in voltage, $V_{bi} = 1$ V; for $V_{bi} = 0$ V, equal anode and cathode work functions of -4.5 eV were used. Selective contacts can be simulated by nullifying the exchange rate of minority carriers at the contacts. As we are interested in the relative effects of gradient compositions on V_{OC}, we refrain from explicitly addressing other factors such as aggregation or injection barrier variation that are known to affect V_{OC} as well.

2. Results

We will first present the results for simulated devices with zero built-in voltage and nonselective contacts. Here, in the absence of vertical composition gradients or steps, there is no preferential current direction since the device is fully symmetric and there will be no net current output, e.g., the pink dot in **Figure 1**a for a homogeneous (50/50) BHJ. In this case, there are two loss channels that add up to 100%, being (geminate and nongeminate) recombination and charge diffusion to the wrong contact. For the used parameters, the latter amounts to just over 50%, as shown in Figure 1b (pink dot). In a bilayer structure (yellow symbols) on the other hand, diffusion of charge carriers to the wrong contact is strongly suppressed as the anode and cathode are only contacted by donor and acceptor material, respectively, and CT at the hetero-interface channels electrons and holes into the
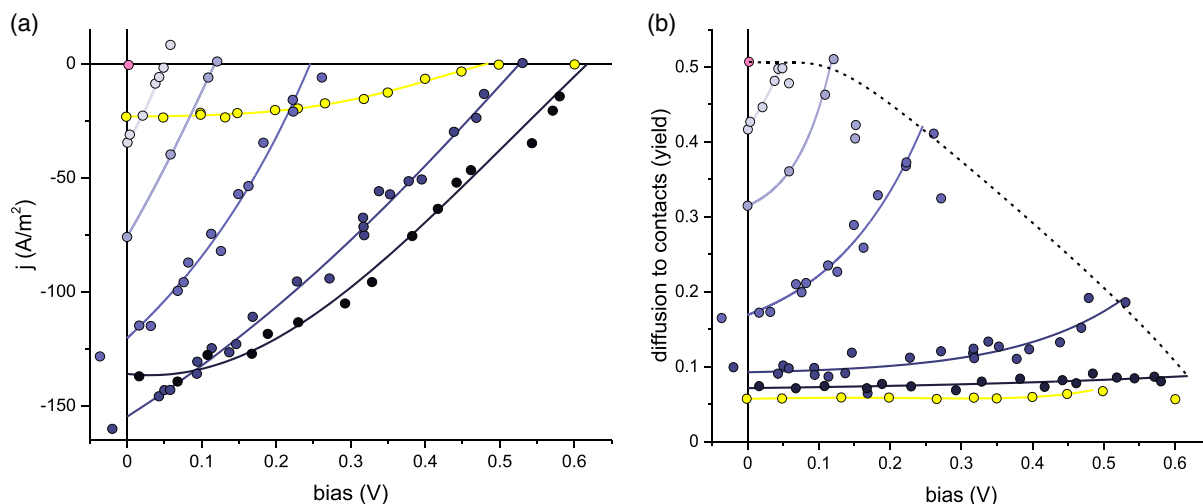
Figure 1. a) Simulated *J–V* curves and diffusion loss to contacts b) at $V_{bi} = 0$ and nonselective contacts, comparing different composition gradients and a bilayer device. Symbols are simulation points; lines are a guide to the eye. The black dashed line in (b) traces the diffusion loss to the contacts for each gradient at V_{OC}. The composition gradient strength increases from 50/50 (no gradient, pink) and 60/40 to 100/0 (light to dark blue). Yellow symbols are for a bilayer device.

acceptor and donor phases, respectively. Note that both charge carriers constituting an exciton can still be collected by a single contact if the exciton is generated close to the semiconductor/contact interface and reaches the contact interface. This loss is included in the diffusion loss, explaining why it is not fully zero for bilayers and the 100/0 gradient composition discussed later. Despite the near-zero diffusion loss, the current density *j* in a bilayer OPV is low as the region around the donor/acceptor interface that effectively contributes to charge generation is narrow, see Figure 1a, which is a common drawback of bilayer OPV.[21]

The BHJ structures on the other hand have a much greater donor/acceptor interface, promoting charge carrier generation. As hypothesized in the introduction, the linear composition gradients direct the diffusion of photocreated holes and electrons to the anode and cathode, respectively. Combined, this leads to a current density that is much higher than for the bilayer and a V_{OC} that is comparable to, and even surpassing, that of the bilayer at stronger gradients, e.g., Figure 1a. Note that the maximum photocurrent for the used parameters equals $j_{max} = qG_0L = 355 \, \mathrm{A \, m^{-2}}$, so at short circuit, an internal quantum efficiency over 40% is reached for optimal gradients, despite the absence of a built-in voltage.

We confirmed that the dropping diffusion losses (Figure 1b) for increasingly steep gradients and the concomitantly increasing current densities are not due to the contact regions becoming increasingly blocking. To investigate up to which gradients' percolation to the contacts is still unhampered, space-charge limited current (SCLC) simulations of unipolar devices were performed as shown in the Supporting Information. Figure S2, Supporting Information, and the corresponding discussion show that contact selectivity due to percolation problems only occurs for 90/10 (and 100/0) gradients; at lesser gradients, no percolation-induced selectivity occurs and the photocurrents and voltages observed in Figure 1a can be attributed to the proposed rectification effect.

To confirm this assignment and to shed further light on the underlying mechanism, we propose a simple analytical expression for the open-circuit voltage, namely

$$V_{OC} = 2 \frac{k_B T_{eff}}{q} \ln\left(\frac{c_{D_0}}{1 - c_{D_0}}\right) \tag{1}$$

Here, k_B is the Boltzmann constant and q the elementary charge. Eq. 1 reflects the "entropic potential difference" between the two ends of the device. It can straightforwardly be derived from the Boltzmann expression $\exp\left(-\frac{q\Delta V_{1,2}}{k_B T_{eff}}\right) = \frac{c_1}{c_2} = \frac{n_1/N_1}{n_2/N_2}$, where $\Delta V_{1,2}$ is the electrostatic potential difference between the two terminals *i* and n_i and N_i are the corresponding carrier and site densities, respectively. Using that having $j = 0$ (at $\Delta V_{1,2} = V_{OC}$) requires, for unselective sink contacts, $n_1 = n_2$ and that $\frac{N_1}{N_2} = \frac{c_{D_0}}{1 - c_{D_0}}$, leads directly to Equation (1). In this simple model, the nonequilibrium nature of the system has been lumped into T_{eff}, the effective temperature of the photocreated charge carrier population in the system. The factor 2 in Equation (1) is to account for both holes and electrons.

As shown in **Figure 2**a, it is possible to properly describe the V_{OC} extracted from kMC simulations with Equation (1) up to ≈75/25 gradients, i.e., $c_{D_0} \approx 0.75$, using $T_{eff} = 728 \, \mathrm{K}$, with the onset of significant deviations roughly coinciding with the onset of contact selectivity as discussed earlier. The reason for the effective temperature strongly exceeding the 300 K lattice temperature is the slow relaxation of the photocreated electron and hole populations.[7,8] The fitted value is in quantitative agreement with the calculated relaxation dynamics, as shown in Figure 2b,c. Data for electrons and holes individually are shown in Figure S3, Supporting Information. The histograms in panel b show that charge extraction typically occurs at around 1×10^{-7} s, speeding up for steeper gradients. The corresponding transient effective temperature has been calculated from the time-dependent mean energy of the charge carrier population $\bar{E}(t)$ via
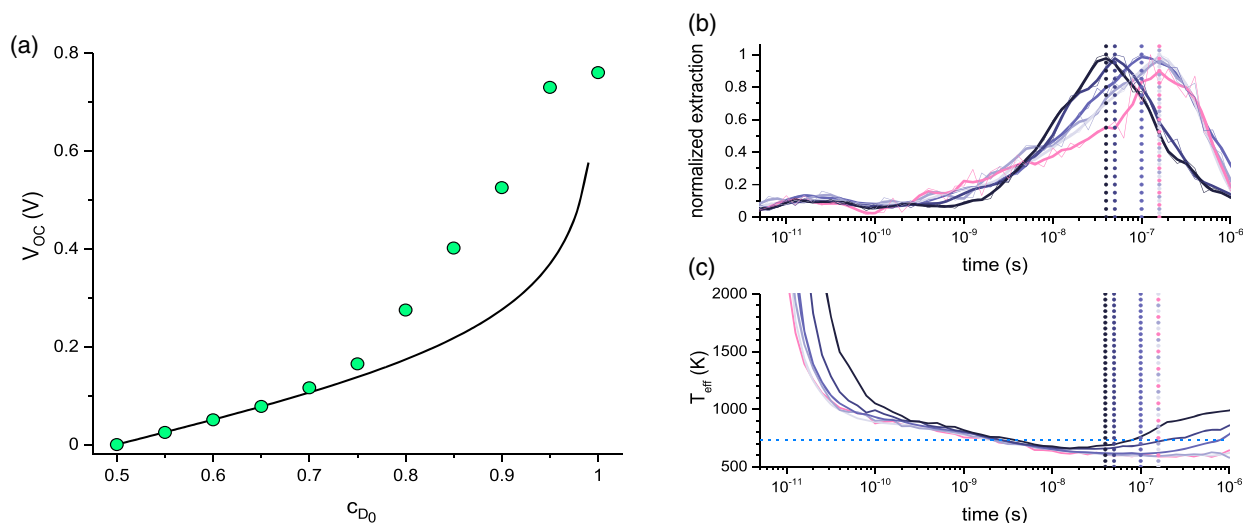
Figure 2. a) V_{OC} versus gradient as characterized by the donor concentration at the anode, c_{D_0}. Dots are obtained from kinetic Monte Carlo simulations ($V_{bi} = 0$ V, e.g., Figure 1), the line is a least-squares fit to Equation (1) up to $c_{D_0} = 0.65$ with fitting parameter $T_{eff} = 728$ K. b) Normalized charge carrier extraction time distribution; thick and thin lines indicate smoothed data and raw data, respectively. c) Corresponding T_{eff} versus time after photogeneration for a homogeneous BHJ (pink), and gradient devices ($c_{D_0} = 0.6$ to 1 in 0.1 steps, light to dark colors). Vertical dashed lines indicate the time at maximum charge carrier extraction; the fitted $T_{eff} = 728$ K from (a) is indicated by the horizontal dashed line in (c).

$$\bar{E}(t) = E_0 \mp \frac{\sigma^2}{k_B T_{eff}} \tag{2}$$

where E_0 is the central energy of the relevant HOMO or LUMO band and t is the time after photocreation.[7] As expected, the thermalization of the carrier population slows down with time, but does not complete, i.e., reach 300 K, within the charge carrier lifetime. The counterintuitive increase in T_{eff} at longer time-scales is due to the preferential extraction of the faster, more mobile carriers, leaving a population of nonthermalized, trapped charges behind. Although we refrain from attempting to define a suitably averaged effective temperature from the data shown in Figure 2c, it is clear that the value $T_{eff} = 728$ K obtained from the fit in panel a, and indicated in panel c by the horizontal dashed line, is consistent with the actual thermalization data.

We would like to emphasize that the open-circuit voltages shown in Figure 1 and 2 cannot be interpreted in the common framework of radiative and nonradiative losses with respect to a CT energy or effective gap.[22] Not only do these quantities not enter in Equation (1) and (2) but also the (transient thermalization of a) far-from-equilibrium charge carrier distribution is fundamentally at odds with the assumption of detailed balance that underlays the conventional interpretation of V_{OC}.[23]

The nonequilibrium mechanism underlying the photocurrents presented so far is further highlighted by the increasing V_{OC} with increasing disorder as shown in **Figure 3**a; an analysis of the corresponding diffusion losses is given in Figure S4, Supporting Information. This behavior is opposite to what one gets from equilibrium models in which V_{OC} decreases with increasing disorder due to increasing thermalization losses.[24] It is, however, consistent with the mechanism proposed here as we find higher effective temperatures with increasing disorder, as shown in Figure 3b. The latter data can in turn be explained by the slower thermalization with increasing disorder.[7] The

T_{eff} values corresponding, via Eq. 1, to the V_{OC} of the $J-V$ curves in panel a are shown in the inset to panel a and their difference of ≈ 400 K corresponds quasi-quantitatively with the vertical distance between the corresponding relaxation transients shown in Figure 3b. The lower absolute values in panel b at time ranges close to maximum charge carrier extraction are consistent with the deviations from Eq. 1 in Figure 2a for large gradients. Although this is not further pursued here, we notice that the kMC model reproduces the common trend of an increase in V_{OC} with decreasing temperature, which is consistent with the notion that the effective temperature is also dependent on lattice temperature, see Figure S5, Supporting Information.[25,26]

Having established that composition gradients can provide substantial photocurrents and photovoltages in systems without built-in voltage, the question remains if any performance increase can be expected for practically relevant systems with finite V_{bi}. In this case, we obtain a proper $J-V$ curve for the BHJ without composition gradient as the symmetry is broken by the built-in voltage, see the pink line and symbols shown in **Figure 4**. Importantly, we find that also in this case, the performance can be significantly increased by incorporating a composition gradient, e.g., blue-colored lines and the inset to panel b. Both fill factor and V_{OC} are increased compared to the homogeneous device, where the latter is increased by almost 0.2 eV. To rule out the voltage increase stemming from low-donor or low-acceptor effects, we performed the same simulations with a reversed 10/90 gradient. The resulting $J-V$ curve (red symbols) has a dramatically reduced V_{OC} as compared to the gradient-free case, showing that the reduced interfacial area does not cause the difference observed between the 50/50 and forward 90/10 gradient devices.[27]

The inset of Figure 4b shows the impact of the gradient composition on simulated output power and efficiency. The latter has been estimated by dividing the output power at a maximum
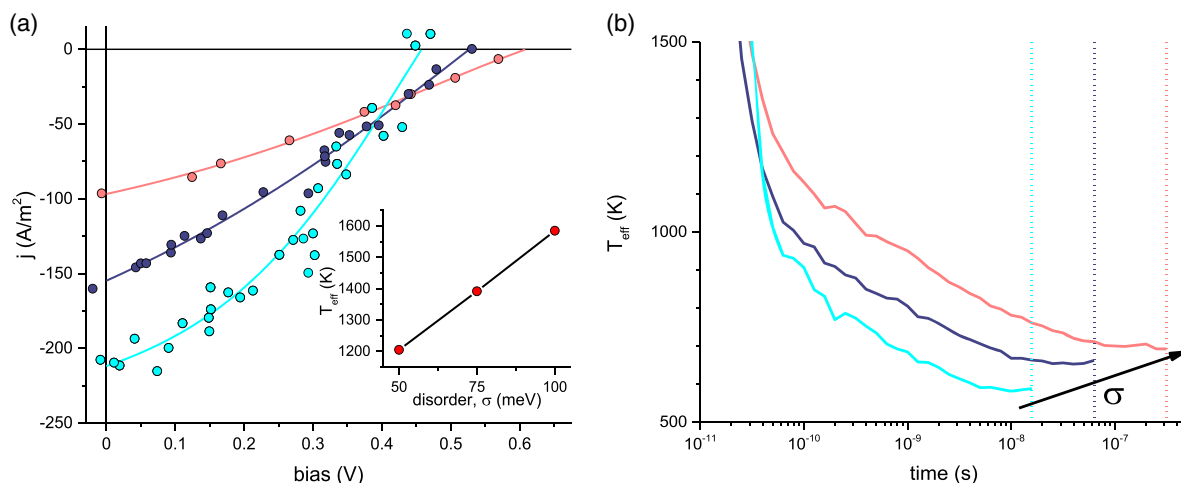
Figure 3. a) Simulated J–V curves for a 90/10 gradient, $V_{bi} = 0$ V and $\sigma_{DOS} = 50$, 75, and 100 meV (light blue, dark blue, and red symbols, respectively). Lines are a guide to the eye. The inset shows T_{eff} derived from V_{OC} via Eq. 1 versus disorder. b) Transient effective temperature versus time after photogeneration from Eq. 2. The dotted vertical lines indicate the typical extraction times.
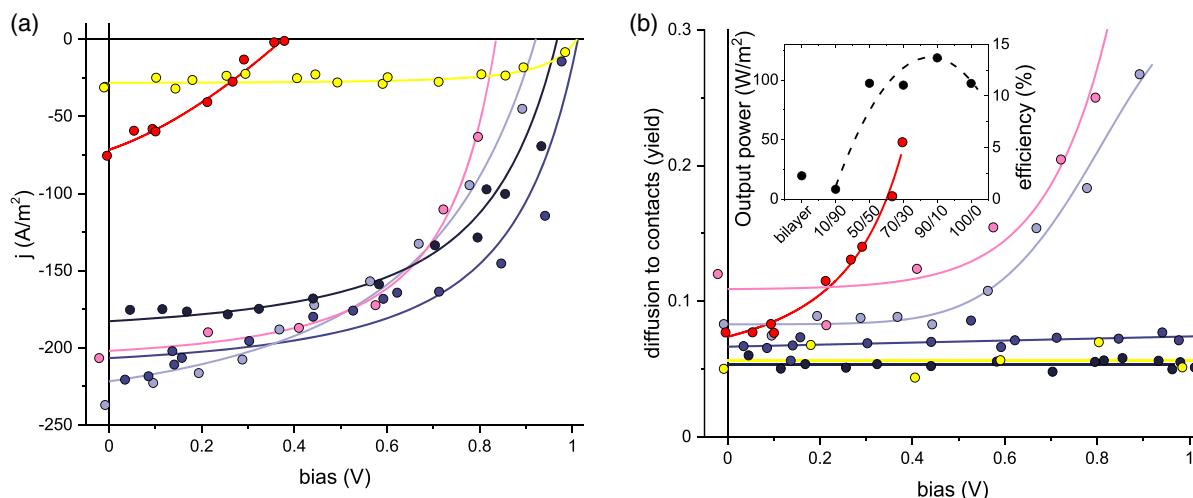

Figure 4. a) J–V curves and diffusion loss to contacts b) at $V_{bi} = 1$ V and nonselective contacts for different BHJ gradients and a bilayer device. Lines are a guide to the eye. The composition gradient variations are 50/50 (no gradient, pink), 70/30, 90/10, and 100/0 (light to dark blue). Yellow symbols are for a bilayer device; red symbols are for a reverse (10/90) gradient, acting opposite to the built-in voltage. The inset plots the simulated maximum output power and associated power conversion efficiency based on the curves in panel (a).

power point by the power associated with the exciton generation in the simulation, i.e., $P_{in} = qE_{gap}G_0L$, where the HOMO–LUMO gap $E_{gap} = 2.0$ eV is used. Note that in this case, the 90/10 gradient is optimal, contrary to the case of zero V_{bi} where 100/0 was better. This we explain by there being a trade-off between reduced charge generation in the strongly depleted contact regions and more directed diffusion at increasing composition gradient. With the added driving force of a built-in voltage, the charge generation loss at the 100/0 gradient outweighs the gain of a more directed diffusion. The bilayer now exhibits a V_{OC} that is equally high as for the optimal gradient, and equal to V_{bi}, but maintains a low current. Figure 4b shows that the reason for the improved performance of the gradient devices as compared to the homogeneous one is, as for the case with $V_{bi} = 0$,

suppressed diffusion loss to the contacts. Especially for 80/20 and steeper gradients, there is no increase in diffusion loss when approaching V_{OC}, whereas devices with less steep or no composition gradient show a steep upswing toward V_{OC} due to the vanishing driving force for directional motion. A detailed analysis of the different loss channels is shown in Figure S6, Supporting Information.

In the pursuit of optimizing OPV, significant effort has been put in developing and understanding charge-selective contacts in the form of hole and electron transport layers (HTL, ETL) to reduce recombination of photocreated charges at the opposite contact.[28–30] **Figure 5** compares a 50/50 BHJ with a 90/10 gradient device, both with $V_{bi} = 1$ V and perfectly selective contacts. Even in this case, a vertical phase composition gradient improves

2000400 (5 of 7)
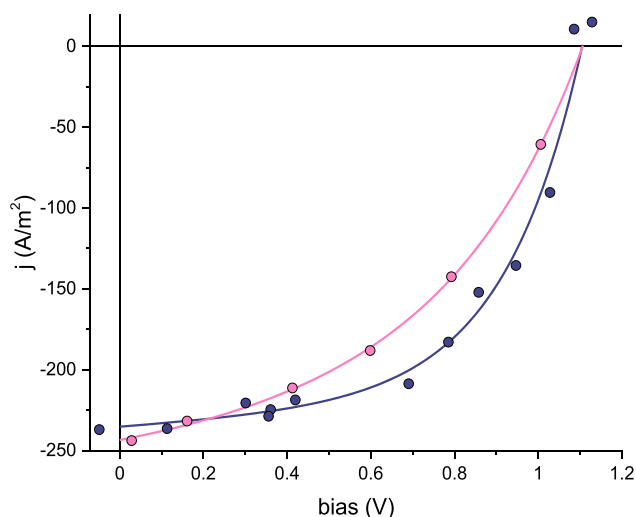
Figure 5. Simulated J–V curves for $V_{bi} = 1\,V$ with selective contacts and gradient 50/50 (pink) and 90/10 (dark blue). Lines are a guide to the eye.

the performance, in this case, mostly in the form of an increased fill factor. The nonequilibrium mechanism underlying the boost in V_{OC} is shown by the fact that, especially for the gradient device, V_{OC} exceeds V_{bi} by $\approx 0.1\,V$, which is impossible in an equilibrium model. Note, in this context that the mere introduction of selective contacts is also expected to lead to an increase in V_{OC}, irrespective of gradient effects or material characteristics.[31]

3. Conclusion

Using nonequilibrium kinetic Monte Carlo simulations, we have shown that suitably chosen vertical composition gradients in the donor:acceptor ratio in organic BHJ solar cells can lead to relevant improvements in device performance. For the used realistic device parameters, improved fill factors and open-circuit voltage increases of up to $\approx 0.2\,V$ are found. The underlying mechanism is the rectification of otherwise undirected and diffusive motion associated with the slow thermalization of photogenerated charge carriers in the Gaussian DOS. A simple analytical model that accounts for the high effective temperature of photogenerated charge carriers corroborates the interpretation. In stark contrast to common equilibrium (drift-diffusion) models, we show that for gradient devices V_{OC} can actually increase with increasing disorder, and even exceed the built-in voltage. Therefore, the performance of OPV devices can be rationally enhanced by treating them as nonequilibrium systems. Particularly, the rectification of thermalization losses may actually prove to be a way to beat the Shockley–Queisser limit, to which we have to add that the SQ limit of OPV is rather negatively affected by the same energetic disorder that enables the effect proposed in this article.

The base value for the energetic disorder, 75 meV, used in this article is rather modest for classic polymer:fullerene systems, though highly relevant for state-of-the-art nonfullerene systems.[32–34] Thus, gradient-engineering of OPV is a plausible

and in principle generally applicable route to improved device performance. However, it is very well possible that unintentional gradients, for example, due to different surface and interfacial energies of the donor and acceptor materials causing a spontaneous stratification during layer deposition, already exist and play a role in optimized OPV systems, as alluded to by several authors, e.g., the Introduction section. At the same time, our modeling shows that rather strong gradients, beyond $\approx 80/20$, are needed to obtain significant boosting of V_{OC} and fill factor. Since too pure phases are prone to hamper efficient charge generation and separation, using the full potential of gradient compositions in actual devices will require careful optimization. We foresee two strategies that can be pursued to this end. First, in binary blends in which the constituent materials have sufficiently heterogeneous and suitably chosen interaction parameters, stratification control has been demonstrated for high-performance organic field effect transistors.[35] Alternatively, or possibly in combination, one can imagine the fabrication of sharp donor:acceptor bilayers, followed by temperature- and time-controlled diffusion during a thermal annealing step.

Finally, we would like to remark that, although not discussed in this article, the gradient mechanism may also drive mesoscale charge separation in D:A interfacial areas in phase-separated BHJ. As such gradients can be expected to be very steep, they might well contribute to the excellent fill factors in recent nonfullerene OPV devices.[36–38]

Supporting Information

Supporting Information is available from the Wiley Online Library or from the author.

Conflict of Interest

The authors declare no conflict of interest.

[1] W. Shockley, H. J. Queisser, *J. Appl. Phys.* **1961**, *32*, 510.
[2] R. T. Ross, A. J. Nozik, *J. Appl. Phys.* **1982**, *53*, 3813.
[3] C. A. Nelson, N. R. Monahan, X.-Y. Zhu, *Energy Environ. Sci.* **2013**, *6*, 3508.
[4] S. Almosni, A. Delamarre, Z. Jehl, D. Suchet, L. Cojocaru, M. Giteau, B. Behaghel, A. Julian, C. Ibrahim, L. Tatry, H. Wang, T. Kubo,

S. Uchida, H. Segawa, N. Miyashita, R. Tamaki, Y. Shoji, K. Yoshida, N. Ahsan, K. Watanabe, T. Inoue, M. Sugiyama, Y. Nakano, T. Hamamura, T. Toupance, C. Olivier, S. Chambon, L. Vignau, C. Geffroy, E. Clouet, et al. *Sci. Technol. Adv. Mater.* **2018**, *19*, 336.

[5] V. Abramavicius, V. Pranculis, A. Melianas, O. Inganäs, V. Gulbinas, D. Abramavicius, *Sci. Rep.* **2016**, *6*, 32914.

[6] P. A. Lane, P. D. Cunningham, J. S. Melinger, O. Esenturk, E. J. Heilweil, *Nat. Commun.* **2015**, *6*.

[7] H. Bässler, *Phys. Status. Solidi. B* **1993**, *175*, 15.

[8] A. Melianas, F. Etzold, T. J. Savenije, F. Laquai, O. Inganäs, M. Kemerink, *Nat. Commun.* **2015**, *6*.

[9] A. Melianas, V. Pranculis, Y. Xia, N. Felekidis, O. Inganäs, V. Gulbinas, M. Kemerink, *Adv. Energy Mater.* **2017**, *7*, 1602143.

[10] W. Tress, K. Leo, M. Riede, *Sol. Energy Mater. Sol. Cells* **2011**, https://doi.org/10.1016/j.solmat.2011.06.003.

[11] B. Beyer, R. Pfeifer, J. K. Zettler, O. R. Hild, K. Leo, *J. Phys. Chem. C* **2013**, *117*, 9537.

[12] L. Chen, Y. Tang, X. Fan, C. Zhang, Z. Chu, D. Wang, D. Zou, *Org. Electron.* **2009**, *10*, 724.

[13] X. Guo, N. Zhou, S. J. Lou, J. Smith, D. B. Tice, J. W. Hennek, R. P. Ortiz, J. T. L. Navarrete, S. Li, J. Strzalka, L. X. Chen, R. P. H. Chang, A. Facchetti, T. J. Marks, *Nat. Photon.* **2013**, *7*, 825.

[14] Y. Wang, B. Wu, Z. Wu, Z. Lan, Y. Li, M. Zhang, F. Zhu, *J. Phys. Chem. Lett.* **2017**, *8*, 5264.

[15] L. Zhang, X. Xing, L. Zheng, Z. Chen, L. Xiao, B. Qu, Q. Gong, *Sci. Rep.* **2015**, *4*.

[16] J. Huang, J. H. Carpenter, C.-Z. Li, J.-S. Yu, H. Ade, A. K.-Y. Jen, *Adv. Mater.* **2016**, *28*, 967.

[17] P. Bi, T. Xiao, X. Yang, M. Niu, Z. Wen, K. Zhang, W. Qin, S. K. So, G. Lu, X. Hao, H. Liu, *Nano Energy* **2018**, *46*, 81.

[18] S. Bi, Z. Ouyang, S. Shaik, D. Li, *Sci. Rep.* **2018**, *8*.

[19] Y. M. Nam, J. Huh, W. H. Jo, *J. Appl. Phys.* **2011**, *110*, 114521.

[20] S. Wilken, T. Upreti, A. Melianas, S. Dahlström, G. Persson, E. Olsson, R. Österbacka, M. Kemerink, *Sol. RRL* **2020**, 2000029.

[21] P. W. M. Blom, V. D. Mihailetchi, L. J. A. Koster, D. E. Markov, *Adv. Mater.* **2007**, *19*, 1551.

[22] D. Qian, Z. Zheng, H. Yao, W. Tress, T. R. Hopper, S. Chen, S. Li, J. Liu, S. Chen, J. Zhang, X.-K. Liu, B. Gao, L. Ouyang, Y. Jin, G. Pozina, I. A. Buyanova, W. M. Chen, O. Inganäs, V. Coropceanu, J.-L. Bredas, H. Yan, J. Hou, F. Zhang, A. A. Bakulin, F. Gao, *Nat. Mater.* **2018**, *17*, 703.

[23] U. Rau, *Phys. Rev. B* **2007**, *76*, 085303.

[24] J. C. Blakesley, D. Neher, *Phys. Rev. B* **2011**, *84*.

[25] K. Vandewal, K. Tvingstedt, A. Gadisa, O. Inganäs, J. V. Manca, *Phys. Rev. B* **2010**, *81*, 125204.

[26] S. Marianer, B. I. Shklovskii, *Phys. Rev. B* **1992**, *46*, 13100.

[27] K. Vandewal, J. Widmer, T. Heumueller, C. J. Brabec, M. D. McGehee, K. Leo, M. Riede, A. Salleo, *Adv. Mater.* **2014**, *26*, 3839.

[28] E. L. Ratcliff, B. Zacher, N. R. Armstrong, *J. Phys. Chem. Lett.* **2011**, *2*, 1337.

[29] O. J. Sandberg, M. Nyman, R. Österbacka, *Phys. Rev. Appl.* **2014**, *1*, 024003.

[30] S. Wilken, J. Parisi, H. Borchert, *J. Phys. Chem. C* **2014**, *118*, 19672.

[31] O. J. Sandberg, J. Kurpiers, M. Stolterfoht, D. Neher, P. Meredith, S. Shoaee, A. Armin, *Adv. Mater. Interfaces* **2020**, *7*, 2000041.

[32] N. Felekidis, A. Melianas, M. Kemerink, *Org. Electron.* **2018**, *61*, 318.

[33] T. Upreti, Y. Wang, H. Zhang, D. Scheunemann, F. Gao, M. Kemerink, *Phys. Rev. Appl.* **2019**, *12*, 064039.

[34] A. Karki, G.-J. A. H. Wetzelaer, G. N. M. Reddy, V. Nádaždy, M. Seifrid, F. Schauer, G. C. Bazan, B. F. Chmelka, P. W. M. Blom, T.-Q. Nguyen, *Adv. Funct. Mater.* **2019**, *29*, 1901109.

[35] K. Zhao, O. Wodo, D. Ren, H. U. Khan, M. R. Niazi, H. Hu, M. Abdelsamie, R. Li, E. Q. Li, L. Yu, B. Yan, M. M. Payne, J. Smith, J. E. Anthony, T. D. Anthopoulos, S. T. Thoroddsen, B. Ganapathysubramanian, A. Amassian, *Adv. Funct. Mater.* **2016**, *26*, 1737.

[36] J. Yuan, Y. Zhang, L. Zhou, G. Zhang, H.-L. Yip, T.-K. Lau, X. Lu, C. Zhu, H. Peng, P. A. Johnson, M. Leclerc, Y. Cao, J. Ulanski, Y. Li, Y. Zou, *Joule* **2019**, *3*, 1140.

[37] Y. Cui, H. Yao, J. Zhang, T. Zhang, Y. Wang, L. Hong, K. Xian, B. Xu, S. Zhang, J. Peng, Z. Wei, F. Gao, J. Hou, *Nat. Commun.* **2019**, *10*.

[38] M.-H. Jao, H.-C. Liao, W.-F. Su, *J. Mater. Chem. A* **2016**, *4*, 5784.

2000400 (7 of 7)